Study on lattice vibrational properties and Raman spectra of Bi_2Te_3 based on density-functional perturbation theory*

Feng Song-Ke(冯松科), Li Shuang-Ming(李双明)†, and Fu Heng-Zhi(傅恒志)

State Key Laboratory of Solidification Processing, Northwestern Polytechnical University (NPU), Xi'an 710072, *China*

(Received 8 August 2013; revised manuscript received 2 April 2014; published online 20 June 2014)

We present a variational density-functional perturbation theory (DFPT) to investigate the lattice dynamics and vibrational properties of single crystal bismuth telluride material. The phonon dispersion curves and phonon density of states (DOS) of the material were obtained. The phonon dispersions are divided into two fields by a phonon gap. In the lower field, atomic vibrations of both Bi and Te contribute to the DOS. In the higher field, most contributions come from Te atoms. The calculated Born effective charges and dielectric constants reveal a great anisotropy in the crystal. The largest Born effective charge generates a significant dynamic charge transferring along the *c* axis. By DFPT calculation, the greatest LO–TO splitting takes place in the infrared phonon modes and reaches 1.7 THz in the Brillouin zone center. The Raman spectra and peaks corresponding to respective atomic vibration modes were found to be in good agreement with the experimental data.

Keywords: density-functional perturbation theory, Bi_2Te_3 material, lattice vibrational properties, Raman spectra

PACS: 63.20.–e, 63.20.D–, 63.20.dk, 78.30.–j **DOI:** 10.1088/1674-1056/23/8/086301

1. Introduction

Bismuth chalcogenide alloys, possessing a special topological layered structure, have drawn numerous research interests in the realm of superconductive, thermoelectric, and thermomagnetic applications.[1–4] Among the chalcogenide compounds, Bi_2Te_3 crystal exhibits a quintuplicate atomic layer in a sequence of Te^1–Bi–Te^2–Bi–Te^1. This topological layered Bi_2Te_3 structure exhibits a lower thermal conductivity but a higher electrical conductivity at room temperature;[5–7] these intrinsic transport properties make it a promising thermoelectric material in a sustainable energy solution.

The topological layered structure of the Bi_2Te_3 material plays a major role in the thermoelectric performance. For instance, the weak Van der Waals bonding between the crystal layers can result in cleavages perpendicular to the *c* axis of the material. Correspondingly, the electrical conductivity along the *c* axis is three times larger than that along the *a* axis.[8] The thermal conductivity along the *c* axis, however, is less than a third of the *a* axis.[9] Being easily exfoliated along the cleavage planes, the resultant single layer of this material has a high electrical conductivity and low thermal conductivity; as a newly formed nanomaterial, this method provides a new route to greatly improve the thermoelectric performance of this compound by the confinement of charge carriers or acoustic phonons.[10–12]

To make a clear image of the above properties dependent on the topological structure of the Bi_2Te_3 crystal, a number of experimental and theoretical studies were presented. The electronic structure of Bi_2Te_3 has been addressed to explain the anisotropic properties in mechanics and electronic transformation.[13] However, from the aspect of atomic lattice vibrations, the anisotropic thermal conduction of Bi_2Te_3 material has not been well understood yet. Previously, Richter *et al.*[14] studied the lattice vibrations of the Bi_2Te_3 crystal and obtained three Raman modes experimentally; but the low-frequency mode E_g^1 has not been observed. Bessas *et al.*[15] have also proved that the crystal phonon dispersion and the phonon density of states cannot be fully described in experiments due to the fact that a perfect single Bi_2Te_3 crystal is hardly obtained.[16,17] Additionally, the unperfected theory modes[18–20] and the half part empirical calculated modes[15,21] have provided a few partial phonon dispersion or the phonon densities of states, but have not provided a clear relationship between the atomic lattice vibrations and the phonon vibration strength in the Bi_2Te_3 crystal. Those theoretical calculations did not yield the knowledge of a great anisotropy in the static dielectric constant and Born effective charge that yield a strong LO–TO splitting at the Brillouin zone center. An accurate description of these lattice dynamic properties will play a significant role in determining the electronic and thermal transport properties.

For these reasons mentioned above, we present a theoretical study of the vibrational properties of bulk Bi_2Te_3 single crystal with the density-functional perturbation theory (DFPT).[22] The theory is the most efficient technique to calculate the phonon frequency of materials.[23–26] It allows the

*Project supported by the National Natural Science Foundation of China (Grant Nos. 50971101 and 51074127) and the Research Fund of the State Key Laboratory of Solidification Processing (NPU) of China (Grant No. SKLSP201010).

†Corresponding author. E-mail: lsm@nwpu.edu.cn

© 2014 Chinese Physical Society and IOP Publishing Ltd

calculation of the crystal response to external electric fields as well as the atomic displacements. The phonon dispersion, phonon density of states, Born effective charges, dielectric constant, LO–TO (longitudinal optical–transverse optical) splitting, and Raman intensities of the Bi_2Te_3 crystal were computed and compared with reported experimental results. The vibrational properties of the Bi_2Te_3 crystal and the anisotropic transport properties in thermal conductivity are addressed to understand the underlying physical mechanisms of phonon transmission in the Bi_2Te_3 crystal.

2. Calculation methods

The crystal structure of Bi_2Te_3 is rhombohedral with the space group $R\bar{3}m$.[27] Bi and Te elements construct a unit cell with three quintuple layers of atoms. As shown in Fig. 1(a), the layers of atoms with a sequence of Te^1–Bi–Te^2–Bi–Te^1 are arranged along the c axis. The lattice parameters, a and c, of Bi_2Te_3 are taken to be 4.38 Å and 30.36 Å, respectively. The first Brillouin zone with five high symmetric points, shown in Fig. 1(b), is used for the first-principle calculation by the Cambridge Serial Total Energy Package (CASTEP).[28]

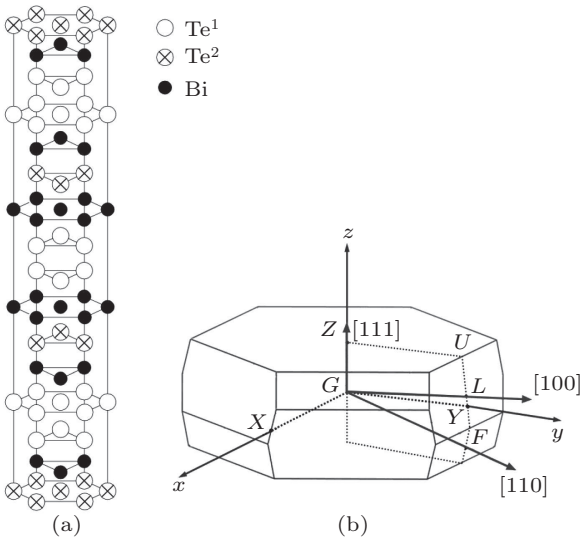


Fig. 1. The crystal structure of Bi_2Te_3 is rhombohedral and constructed with three quintuple layers of atoms. Each quintuple layer is arranged along the c axis in a sequence of Te^1–Bi–Te^2–Bi–Te^1 (a). Five high symmetric points and three axes are plotted in the first Brillouin zone (b). Here, the binary axis (2-fold rotation symmetry) is along x, the bisectrix axis (in the reflection plane) is along y, and the trigonal axis (inversion 3-fold rotation symmetry) is along z.

The norm-conversing pseudopotentials for Te and Bi atoms were taken for electron–ion interactions in pseudo-atomic calculation.[29] The wave function was expanded by using plane waves. The local density approximation with the Ceperley–Alder–Perdew–Zunger functional[30] was applied to evaluate exchange–correlation energy. The cut-off energy of atomic wave functions was set as 500 eV. The Broyden–Fletcher–Goldfarb–Shanno method[31] was employed to relax the lattice parameters and atomic internal coordinates. Sampling of the irreducible wedge of the Brillouin zone (BZ) was generated by the regular Monkhorst-pack grid of $8 \times 8 \times 8$ (60 k points).[13] The predetermined convergence tolerance was set as the root mean square (RMS) force below 0.01 eV/Å, max displacement under 5×10^{-4} Å, max stress less than 0.02 GPa, and energy change less than 1×10^{-6} eV/atom.

For the phonon dispersion evaluation, the density functional perturbation theory was used to compute the atomic vibrational properties. The interatomic force constants of the crystal dynamical matrices were calculated by means of the Fourier interpolation technique with a q-mesh 0.03 $Å^{-1}$ and used to plot the phonon densities of states and phonon dispersion. At the G point, the infrared (IR) and Raman active modes were distributed by using the group theory. Four q points in the vicinity of the BZ center at different directions were taken to calculate the vibrational frequencies, Born-effective charge, and dielectric tensor.

3. Results and discussion

3.1. Phonon dispersion

Figure 2 shows the phonon dispersion curves along the high symmetry directions of the Brillouin zone from the Fourier interpolation and dynamic matrix calculation. The right side of the figure displays the partial density of phonon states (PDOS). It is noted that the calculated unit cell of Bi_2Te_3 crystal contains five atoms. That is, there are three acoustic phonon branches and 12 optical phonon branches. The low-energy vibrations of Bi and Te atoms contribute to the three acoustic branches and the first three low-frequency optical branches, presenting a mixed character of these six low-frequency modes. The rest of the high-frequency optical branches are mainly determined by the vibration of Te atoms that contribute to 80% vibration amplitude.

Another finding is the phonon modes in the GZ direction displaying much lower phonon dispersion. Here, the GZ direction is the c axis ([111] direction of crystal). Along the c axis, there exists a weak coupling between the adjacent Te layers, leading to a small dispersion of phonons in the Bi_2Te_3 crystal. For the experimental evidence, such a small dispersion of phonons can be clearly observed in the weak coupling layers of graphite[32] and BiTeCl[33] materials. As shown in Fig. 2, the low-frequency acoustic branches match well with the experiment data[34] and they play a main role in the thermal conduction of Bi_2Te_3 crystal. The high-frequency phonon branches, possessing lower group velocity, contribute less to the thermal conduction.[35] Additionally, the phonon modes are separated into low phonon modes and high ones due to the difference in atomic mass, producing a band gap between the three lower optical branches and the higher optical ones.

Those lower-frequency phonon modes, expect for the intrinsic three-phonon scattering, can be highly scattered by the defects in the crystal, minifying the lattice thermal conduction efficiently.[36]

To further illustrate the phonon properties of the Bi_2Te_3 crystal, the phonon density of states (DOS) is plotted in Fig. 3. This DOS is based on DFPT calculation with a smearing width of 0.1 THz. The calculated cutoff frequency is 4.56 THz, matching well with the values of 4.5 THz measured by Rauh *et al.*[34] and 4.35 THz calculated by Qiu *et al.*[21] In addition, the calculated DOS in this paper can successfully produce the positions of the peaks, as in Fig. 3, and provide accessible data for the phonon thermal conductivities.[37]

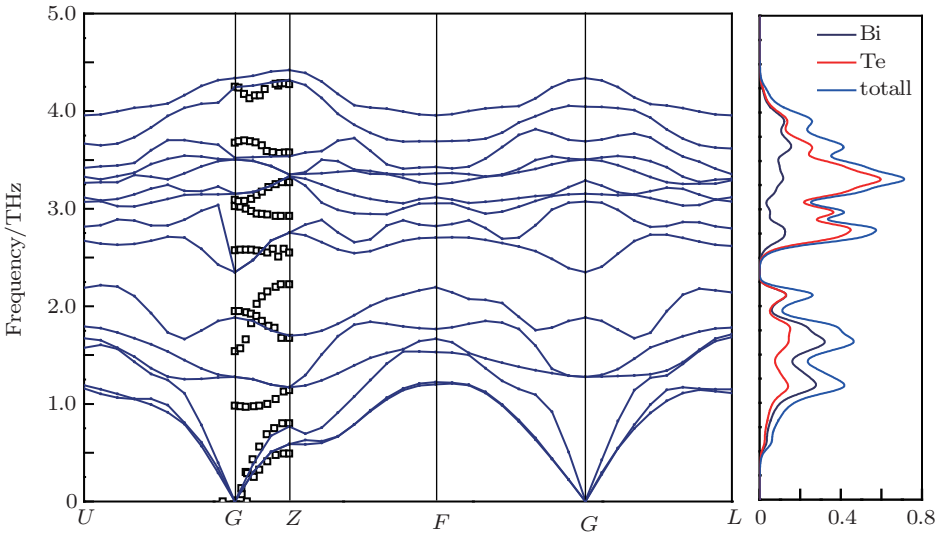


Fig. 2. (color online) Phonon dispersion curves of Bi_2Te_3 at the high symmetry points and the partial density of phonon states (PDOS) is shown at the right side. The square point along the *GZ* direction is the experimental data.[34]

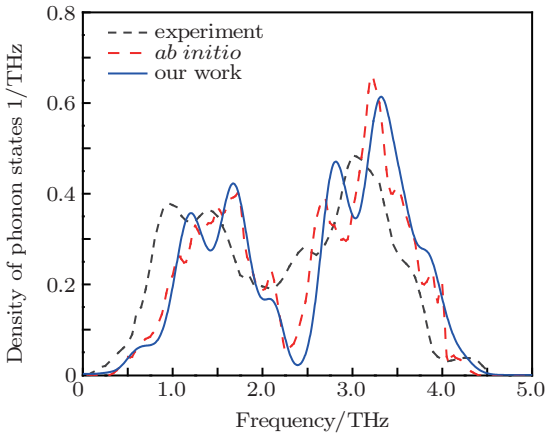


Fig. 3. (color online) Calculated phonon density of states for Bi_2Te_3 crystal, together with the *ab initio* calculation[21] and experimental data.[34]

3.2. Phonons at *G* point

The lattice dynamic properties in bismuth telluride are fully comprehended, expecting to understand the phonon dispersion. The indispensable knowledge of LO–TO splitting of the BZ center optical modes is needed by means of calculating the non-analytic contribution to the dynamic matrix. The knowledge of how to dealt with the non-analytic term is provided by the Born-effective tensor $Z^*_{\alpha\beta}(i)$ and the dielectric tensor $\varepsilon^{\infty}_{\alpha\beta}$. At the BZ center *G* point, Born-effective tensor $Z^*_{\alpha\beta}(i)$[24] is given as:

$$Z^*_{\alpha\beta}(i) = \Omega \frac{\delta P_\alpha}{\delta u_i^\beta (q=0)}\bigg|_{E=0}, \tag{1}$$

where i represents the i-th atom, Ω the volume of the unit cell, δP_a the first-order polarization of the position vector a, and δu_i^β the first-order change of the position vector β of the i atom. Due to the crystal symmetry of Bi_2Te_3, the tensors are diagonal with only two independent parameters and are labeled parallel ($\|$) and perpendicular ($\perp$) to the c axis.

Table 1 shows the magnitude of Born-effective charge tensors $Z^*_{\alpha\beta}(i)$ of the Bi_2Te_3 crystal calculated from Eq. (1). A large anisotropy of Born-effective charge tensors emerges in both $Z^*_{\|}(i)$ and $Z^*_{\perp}(i)$. The ratios of $Z^*_{\|}(i)/Z^*_{\perp}(i)$ are over unit and the maximum corresponding to Te^1 atom reaches 4.461, indicating that the electronic aggregations are different in these two directions. As a result, a significantly dynamic charge transfer takes place along the c axis. This charge transmission anisotropy has been verified in the experiment that demonstrates the electron conductivity perpendicular to the c axis being one third of the one at the parallel direction.[8]

In addition, we also observe a strong correlation between the effective charge $Z^*_{\alpha\beta}(i)$ and atomic positions. For example, Te^1 belongs to the Wyckoff site of 3*a* and Te^2 is 6*c*. The values of $Z^*_{\|}(Te^1)$ and $Z^*_{\|}(Te^2)$ are -4.28304 and -6.02926, respec-

tively. As shown in Table 1, it reveals another strong correlation displaying between $Z^*_{\parallel}$(Bi) and $Z^*_{\parallel}$(Te^2). This correlation can be attributed to the fact that the displacement between Bi and Te^2 modulates the Bi–Te^2 bond parallel to the c axis.

Table 1. The calculated values of independent atomic Born-effective charge $Z^*_{\alpha\beta}(i)$ and the dielectric tensor $\varepsilon^{\infty}_{\alpha_\beta}$. The subscript $\parallel$ and $\perp$ represent the component parallel and perpendicular to the c axis, respectively.

	Born-effective charge			Dielectric tensor	
	Bi	Te^1	Te^2		
$Z^*_{\parallel}$	7.29767	–4.28304	–6.02926	$\varepsilon_{\parallel}$	39.07842
$Z^*_{\perp}$	3.58873	–0.96075	–5.25597	$\varepsilon_{\perp}$	30.1409
$Z^*_{\parallel}/Z^*_{\perp}$	2.034	4.461	1.147	$\varepsilon_{\parallel}/\varepsilon_{\perp}$	1.2965

Another parameter, the dielectric tensor $\varepsilon^{\infty}_{\alpha_\beta}$, also exhibits the anisotropy in the Bi_2Te_3 crystal. In Table 1, the value of $\varepsilon_{\parallel}/\varepsilon_{\perp}$ reaches 1.2965. This value is first reported by the theoretical calculation and no experimental data are available. Previous research work has pointed out that the dielectric constants of Bi_2Te_3 alloy play a critical role in growing micro or nanoscale Bi_2Te_3 particles and film from the solution.[38] For this aspect, our calculated results may provide a mechanism to elucidate the formation of stable Bi_2Te_3 particles and films.

Table 2. The calculated frequencies of the optical phonon branches with their infrared and Raman activities at the BZ center G point. The unit of frequency is in THz.

Mode	Frequency	IR active	Raman active	TO/LO
E^1_g	1.26	–	Y	TO
A^1_g	1.88	–	Y	LO
E^1_u	2.35	Y	–	TO
E^2_u	3.15	Y	–	TO
E^2_g	3.51	–	Y	TO
A^1_u	3.52	Y	–	LO
A^2_u	4.04	Y	–	LO
A^2_g	4.33	–	Y	LO

Table 2 gives the optical phonon branches with infrared (IR) and Raman activities at the G point. The BZ center phonon frequencies of the Bi_2Te_3 crystal are calculated using linear response formalism. The LO–TO splitting of the BZ center was estimated on its non-analytic contribution to the dynamic matrix. The calculation results indicate that all the optical phonons belong to infrared or Raman activities. Two optical modes belong to A_1 and the other two to A_2, and eight to E, where E mode is twofold-degenerate, including IR and Raman-active modes. In these 12 optical modes, there are four LO modes and four doubly degenerate TO modes and no relationship between the TO and LO modes through the eigenvector analysis. This finding matches well with the reported result by Rauh *et al.*[34] As listed in Table 2, LO–TO splittings are observed for the infrared-active modes at the BZ center. The maximum value of A^1_u minus E^1_u reaches 1.17 THz. This large LO–TO splitting value is due to the large $Z^*_{\parallel}$ effective charge and dielectric tensors $\varepsilon_{\parallel}$ in the crystal. The phonon spectrum splitting in the high symmetry points is also calculated. The LO modes of both IR and Raman-active branches are splitting at the G and Z points.

3.3. The Raman analysis

The Bi_2Te_3 crystal belongs to the space group of D^5_{3d} and assumes hexagonal close-packed atomic layers. As shown in Fig. 1(b), it possesses one trigional axis parallel to the c axis and three binary axes perpendicular to the c axis. There are three mirror planes that include the trigonal axis and perpendicular to the binary axis, and one center of inversion with a Te^2 atom in the crystal. On the basis of the group theory and symmetry analysis, the optical modes in the Bi_2Te_3 crystal are divided as $\Gamma_{\rm opt} = 2\Gamma^+_1(\mathrm{R}) + 2\Gamma^+_3(\mathrm{R}) + 3\Gamma^-_1(\mathrm{I}) + 3\Gamma^-_3(\mathrm{I})$ at the center of the Brillouin zone, where R and I represent the Raman and infrared active, respectively. The 12 optical branches belong to $2A_g$, $2E_g$, $2A_u$, and $2E_u$ symmetry, where A, E, g, and u are out-plane lattice vibrations, in-plane lattice vibrations, Raman-active modes, and IR-active modes, respectively.

By aiding the DFPT calculation at the Brillouin zone center, the results of Raman eigenwavenumbers of phonon modes and the displacements of atoms were obtained. Figure 4 shows the Raman frequency of Bi_2Te_3 crystal. There are four peaks of wave, and the maximum eigenwavenumber reaches 134.7 cm^{-1}. The rest of the Raman eigenwavenumbers are given in Table 3, together with previously calculated and experimental data.[39] The theoretical calculation result of E^1_g is 42.3 cm^{-1}, close to the measured value of 38.9 cm^{-1} by Shahil *et al.*[11] but it is lower than 50.6 cm^{-1} reported by Richter *et al.*[14] For higher Raman-active modes, e.g., A^1_{1g}, E^2_g, and A^2_{1g}, the calculated eigenwavenumbers fit well with the experimental data as shown in Table 3.

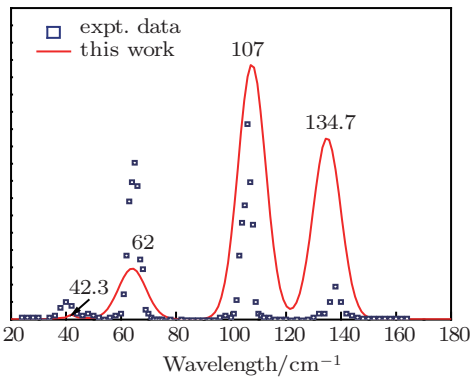


Fig. 4. (color online) The Raman curve of Bi_2Te_3 crystal together with experimental data.[39]

Table 3. The calculated Raman wavenumber peaks in Bi_2Te_3 and other experimental and calculation results. All the wavenumbers are in units of cm^{-1}.

E^1_g	A^1_{1g}	E^2_g	A^2_{1g}	Comments
38.9	61.3	101.3	133.0	nano film[a]
36.5	62.0	102.3	134.0	bulk[b]
50.6	71.1	118.5	128.3	calc. bulk[c]
42.3	62.0	107.0	134.7	our work

[a]Ref. [11]. [b]Ref. [39]. [c]Ref. [22].

A Raman wavenumber peak is related to a specific atom vibration. Figure 5 gives the E_g and A_g modes vibrating in the form of in-phase and out-of-phase. For the E_g^1 mode, the upper two layers of Bi and Te atoms vibrating in the same direction make a greater atomic displacement and produce a lower phonon frequency. For the A_{1g}^1 mode, both Bi and Te atoms vibrating in opposite directions with a short displacement induce a higher frequency (107 cm^{-1}). As for the A_g modes vibrating out of phase, the bonding of each neighboring atom is stronger than that of the E_g modes. As a result, the atomic vibration displacement of A_g modes is restricted and the atomic vibrational frequency of A_g modes is stronger than that of E_g modes. For example, the frequency of A_{1g}^2 is 134.7 cm^{-1}, nearly one half larger than that of E_g^2 mode. The change in phonon frequency exerted by the difference in atomic vibrations will directly enhance the anisotropy in the lattice thermal conduction of the crystal.

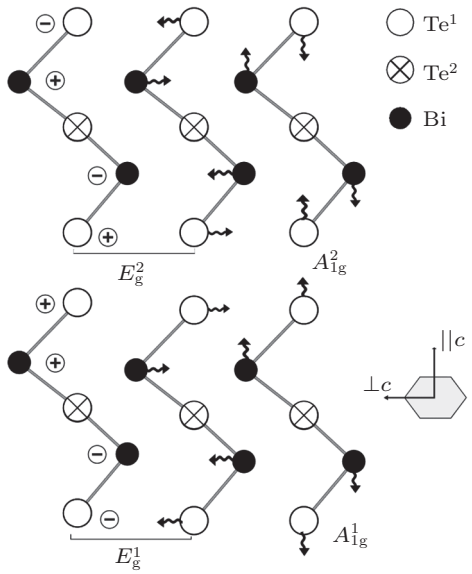


Fig. 5. Atomic displacements of five atoms for double E_g modes in Bi_2Te_3 crystal are 42.3 cm^{-1} and 107.0 cm^{-1} and double A_g modes are 62.0 cm^{-1} and 134.7 cm^{-1}.

The low-frequency phonons emerge at different frequencies along the three axes in the Bi_2Te_3 crystal that dominate the heat conduction of the crystal. Even they are hardly scattered by the point defects in the solid but can be scattered by the boundaries of crystal because the free path lengths for the phonons vary strongly with the vibrational frequency.[40–42] So the topological structure of the Bi_2Te_3 crystal, the E and A modes vibrating in forms of in-phase and out-of-phase, which result in different phonon frequencies, i.e., the dissimilar free path length of the phonons, generating the lattice conductivity parallel to the c axis, is approximately 2–2.5 times smaller than that of the perpendicular direction.[21,43] This anisotropic lattice thermal conduction in the Bi_2Te_3 crystal is enhanced from the phonon vibration modes. It can be used to design and search for high performance thermoelectric materials with lower thermal conductivity.

4. Conclusions

Density-functional perturbation theory calculations have been applied to study the vibrational properties of binary Bi_2Te_3 thermoelectric material. The calculated dispersion curve of the material indicates that the phonon vibrational spectra can be divided into lower active phonon modes and higher ones. The lower phonon modes are attributed to the atomic vibrations of Bi and Te atoms, dominating the conduction of heat in the Bi_2Te_3 crystal. The Boren-effective charges and dielectric tensors reveal that the topological structure of the crystal leads to a strong anisotropy in the directions perpendicular and parallel to the c axis. The obtained large $Z_{\|}^*$ effective charge and dielectric tensors $\varepsilon_{\|}$ show a great LO–TO splitting at the center of the Brillouin zone. The calculation results are in good agreement with the previously reported experimental data. The density-functional perturbation theory is proved to be a practical method which can successfully predict the atomic vibration properties and Raman spectra of the Bi_2Te_3 material.

Acknowledgments

The authors would like to thank Prof. Xu Lei for his suggestions on our manuscript. The calculations have been performed at the Center for High Performance Computing of NWPU.

References

[1] Moore J 2009 *Nat. Phys.* **5** 378
[2] Ning W, Du H F, Kong F Y, Yang J Y, Han Y Y, Tian M L and Zhang Y H 2013 *Sci. Rep.* **3** 1
[3] Zhang C, Sun L, Chen Z Y, Zhou X J, Wu Q, Yi W, Guo J, Dong X L and Zhao Z X 2011 *Phys. Rev. B* **83** 140504
[4] Mehta R J, Zhang Y L, Karthik C, Singh B, Siegel R W, Borca-Tasciuc T and Ramanath G. 2012 *Nat. Mater.* **11** 233
[5] Satterthwaite C B and Ure R W 1957 *Phys. Rev.* **108** 1164
[6] Goldsmid H J 1961 *J. Appl. Phys.* **32** 2198
[7] Snyder G J and Toberer E S 2008 *Nat. Mater.* **7** 105
[8] Nassary M M, Shaban H T and El-Sadek M S 2009 *Mater. Chem. Phys.* **113** 385
[9] Goldsmid H J 1958 *Proc. Phys. Soc.* **72** 17
[10] Teweldebrhan D, Goyal V, Rahman M and Balandin A 2010 *Appl. Phys. Lett.* **96** 053107
[11] Shahil K M F, Hossain M Z, Teweldebrhan D and Balandin A A 2010 *Appl. Phys. Lett.* **96** 153103
[12] Teweldebrhan D, Goyal V and Balandin A 2010 *Nano Lett.* **10** 1209
[13] Wang G F and Cagin T 2007 *Phys. Rev. B* **76** 075201
[14] Richter W and Becker C R 1977 *Phys. Status Solidi B* **84** 619
[15] Bessas D, Sergueev I, Whille H C, Perbon J, Ebling D and Hermann R P 2012 *Phys. Rev. B* **86** 224301
[16] Hashibon A and Elsässer C 2011 *Phys. Rev. B* **84** 144117

[17] Rowe D M 1995 *CRC Handbook of Thermoelectrics* (Florida: CRC Press) Chap, 9, pp. 8–12

[18] Kullmann W, Eichhorn G, Rauh H, Geick R, Eckold G and Steigenberger U 1990 *Phys. Status Solidi* **162** 125

[19] Wagner V, Dolling G, Powell B M and Landweher G 1978 *Phys. Status Solidi* **85** 311

[20] Jenkins J O, Rayne J A and Ure R W J 1972 *Phys. Rev. B* **5** 3171

[21] Qiu B and Ruan X L 2009 *Phys. Rev. B* **80** 165203

[22] Gonze X and Lee C 1997 *Phys. Rev. B* **55** 10355

[23] Baroni S, De G S, Dal C A and Giannozzi P 2001 *Rev. Mod. Phys.* **73** 515

[24] Zhou B, Qing S and He D Y 2009 *Chin. Phys. B* **18** 4988

[25] Liu B, Gu M, Liu X L, Huang S M, Ni C, Li Z R and Wang R B 2010 *Chin. Phys. B* **19** 26301

[26] Miao L, Liu H J, Hu Y, Zhou X, Hu C Z and Shi J 2010 *Chin. Phys. B* **19** 16301

[27] Taylor R E, Leung B, Lake M P and Bouchard L S 2012 *J. Phys. Chem. C* **116** 17300

[28] Segall M D, Philip J D L, Probert M J, Pickard C J, Hasnip P J, Clark S J and Payne M C 2002 *J. Phys.: Condens. Matter* **14** 2717

[29] Medlin D L, Ramasse Q M, Spataru C D and Yang N Y C 2010 *J. Appl. Phys.* **108** 043517

[30] Perdew J P and Zunger A 1981 *Phys. Rev. B* **23** 5048

[31] Pfrommer B G, Côté M, Louie S G and Cohen M L 1997 *J. Comput. Phys.* **131** 233

[32] Wirtz L and Rubio A 2004 *Solid State Commun.* **131** 141

[33] Sklyadneva I Y, Heid R, Bohnen K P, Chis V, Volodin V A, Kokh K A, Tereshchenko O E, Echenique P M and Chulkov E V 2012 *Phys. Rev. B* **86** 094302

[34] Rauh H, Geick R, Kohler H, Nucker N and Lehner N 1981 *J. Phys. C: Solid State Phys.* **14** 2705

[35] Goldsmid H J 2009 *Introduction to Thermoelectricity* (Heidelberg: Springer) p. 70

[36] Chernatynskiy A and Phillpot S R 2013 *Curr. Opin. Solid State Mater. Sci.* **17** 1

[37] Broido D A, Malorny M, Birner G, Mingo N and Stewart D A 2007 *Appl. Phys. Lett.* **91** 231922

[38] Nguyen H P, Wu M X, Su J, Vullers R J M, Vereecken P M and Fransaer J 2012 *Electrochim. Acta* **68** 9

[39] Kullmann W, Geurts J, Richter W, Lehner N, Rauh H, Steigenberger U, Eichhorn G and Geick R 1984 *Phys. Status Solidi B* **125** 131

[40] Chen G, Zeng T, Borca T T and Song D 2000 *Mater. Sci. Eng. A* **292** 155

[41] Koh Y K and Cahill D G 2007 *Phys. Rev. B* **76** 075207

[42] Minnich A J, Dresselhaus M S, Ren Z F and Chen G 2009 *Energ. Environ. Sci.* **2** 466

[43] Jacquot A, Bayer B, Winkler M, Böttner H and Jaegle M 2012 *J. Solid State Chem.* **193** 105